Impact of chemically grown silicon oxide interlayers on the hydrogen distribution at hydrogenated amorphous silicon/crystalline silicon heterointerfaces

Kazuhiro Gotoh[1,*], Markus Wilde[2], Shohei Ogura[2], Yasuyoshi Kurokawa[1], Katsuyuki Fukutani[2], and Noritaka Usami[1]

[1] *Department of Materials Process Engineering, Graduate School of Engineering, Nagoya University, Furo-cho, Chikusa-ku, Nagoya 464-8603, Japan*

[2] *Institute of Industrial Science, The University of Tokyo, 4-6-1, Komaba, Meguro-ku, Tokyo 153-8505, Japan*

*Corresponding author

E-mail address: gotoh.kazuhiro@material.nagoya-u.ac.jp (K. Gotoh)

ABSTRACT

We studied the impact of oxidizing pre-treatments (OPT) and post deposition annealing (PDA) on the passivation performance and the hydrogen distribution near the interface between crystalline silicon (c-Si) and hydrogenated amorphous silicon (a-Si:H), the critical functional region in Si heterojunction solar cells. The OPT prior to deposition of the a-Si:H layer consists of immersing the c-Si substrates into hydrogen peroxide solutions, which forms a silicon oxide interlayer. Spectroscopic ellipsometry (SE) indicates that slightly thicker a-Si:H layers result from OPT. The refractive index and the extinction coefficient are increased by inserting the oxide interlayers, suggesting that less deficient and denser a-Si:H layers can be formed. Under optimum conditions, OPT leads to at least 2-fold improvement of the effective photo-generated carrier lifetime. PDA at 200 ºC further improves the passivation performance of samples with an interlayer. Hydrogen profiling with nuclear reaction analysis clarifies that higher hydrogen concentrations are present around the heterointerfaces of samples with an interlayer and that these hydrogen concentrations are maintained after PDA. Our results suggest that the oxide interlayer can suppress hydrogen desorption in the initial growth stage of high-quality a-Si:H layers and during subsequent PDA, resulting in excellent passivation performance.

Keywords

Oxidizing pre-treatment, passivation, hydrogen distribution, hydrogenated amorphous silicon, crystalline silicon.

1. Introduction

Extremely high conversion efficiency exceeding 25% is achieved by crystalline silicon (c-Si) heterojunction solar cells using hydrogenated amorphous Si (a-Si:H) due to its highly effective passivation of the c-Si surface [1-4]. The outstanding passivation effect on the c-Si surface by intrinsic type a-Si:H (i-a-Si:H) leads to a high open circuit voltage (V_{OC}) owing to larger quasi Fermi energy splitting by accumulation of photogenerated carriers in c-Si [5-7]. A high quality a-Si:H thin layer is essential for the remarkable passivation performance, since electrically active defects, i.e. dangling bonds and nano-voids, around the a-Si:H/c-Si heterointerface and in the bulk of a-Si:H are detrimental [6]. The interface defect density depends on the density of interfacial dangling bonds and determines the carrier recombination rate [8-10]. It is reported that i-a-Si:H layers with few electrically active defects are achievable at a moderate growth temperature which results in excellent passivation performance [11], whereas crystallization of a-Si:H at higher temperatures may ruin the a-Si:H/c-Si interface [11-13]. Thus, crystallization of the a-Si:H layer should be averted to obtain a high V_{OC}. Inserting an ultrathin silicon oxide (SiO_x) interlayer between a-Si:H and c-Si by dipping the c-Si substrates into oxidizing chemicals prior to a-Si:H deposition is another possible way to prevent the detrimental epitaxial growth of Si:H on c-Si [14-16].

It is well known that interfacial passivation mechanisms consist of terminating dangling bonds at the Si surface (often addressed as chemical passivation) and controlling the population of electrons and holes by electrical fields (so-called field effect passivation) [17]. For the i-a-Si:H/c-Si heterojunction, it is considered that the passivation effect is dominantly caused by hydrogenation of Si dangling bonds [17-23]. Therefore, the hydrogen distribution near the a-Si:H/c-Si interface is crucially important, and a deeper understanding of the prominent passivation effect of a-Si:H may enable further improvement of the device performance. Recently, we clarified the effect of the deposition temperature on the correlation between

hydrogen near the a-Si:H/c-Si interface and the passivation performance by nuclear reaction analysis (NRA) [11]. The NRA technique uses MeV-^{15}N ions as probes to non-destructively reveal the hydrogen depth distribution in samples on a nanometer scale [24-26]. It was shown earlier that the oxidizing pre-treatment (OPT) is successful in obtaining excellent passivation performance [14], yet the distribution of interfacial hydrogen in OPT a-Si:H/c-Si systems has still remained unrevealed.

In this work, we therefore studied the influence of ultrathin SiO_x interlayers on the hydrogen distribution and on the electrical and optical properties of a-Si:H/c-Si heterojunctions. For the chemical oxidation pre-treatment, we dipped the c-Si substrates into hydrogen peroxide solutions with different concentrations for various periods of time. The physical thickness and optical properties of the fabricated a-Si:H/c-Si heterojunctions were characterized by spectroscopic ellipsometry (SE), and their passivation performance was evaluated with photoconductance measurements. The near-interfacial H distributions were revealed with NRA. The impact of post deposition annealing (PDA) at 200 °C on the H distributions and passivation performance was also studied, which provided essential information on the possible origin of the passivation performance enhancement by the oxide interlayer.

2. Experimental methods

Double side mirror-polished, floating zone (Fz) grown, 280 μm thick n-type c-Si(100) substrates were cleaned by Semicoclean-23 (Furuuchi Chemicals) for 6 minutes in an ultra-sonic bath. The native surface oxide layer was then removed by immersing the substrates into 2.5% HF for 1 minute followed by dipping into ozonized and deionized water (DI-O_3) for 10 minutes to clean the surface and to form a protective oxide layer [27-29]. The ozone concentration in the DI-O_3 was about 25 ppm. After the protective oxide layer was stripped off by 2.5% HF, the OPT was performed by dipping the substrates into H_2O_2 solutions with

different concentrations for various periods of time. Subsequently, the substrates were quickly loaded into a chamber for plasma enhanced chemical vapor deposition (PECVD) with a frequency of 27.12 MHz (ULVAC Inc., CME-200J). Intrinsic type a-Si:H (i-a-Si:H) and n-type a-Si:H (n-a-Si:H) were deposited at a c-Si substrate temperature of 180 °C for passivation and electrical measurements, respectively. The n-a-Si:H is used to improve contact with aluminium electrodes and to prevent reaction between the i-a-Si:H layers and the Al electrodes. The total pressure and RF power density were fixed at 25 Pa and 32.5 mW/cm^2, respectively. To deposit i-a-Si:H, silane gas with flow rate of 40 sccm was used. For deposition of n-a-Si:H, a gas mixture of silane, hydrogen and 1% phosphine diluted in H_2 was employed with respective flow rates of 40, 380, and 20 sccm. Aluminium electrodes were deposited on the front n-a-Si:H side and the rear c-Si side by vacuum evaporation in order to characterize the electrical resistance. PDA was performed in air using a hot plate at 200 °C for 30 min. These PDA temperature and duration parameters are chosen following commonly employed conditions in the metallization process of SHJ solar cell fabrication by screen printing [30,31].

The a-Si:H layer thickness, refractive index (n) and extinction coefficient (k) were analyzed by spectroscopic ellipsometry (SE, J. A. Woollam Co., M-2000DI-Nug). For modeling the a-Si:H layer, the Tauc-Lorentz model (the product of the Tauc gap and a Lorentz model) was employed [32,33]. Native oxide and silicon oxide interlayers were taken into account (Supporting Information Figure S1). To model the silicon oxide layers, the dielectric function was determined by analysing chemically grown silicon oxide on c-Si by H_2O_2 solutions with different concentration and time. The Sellmeier approximation was used to model the dielectric function of the silicon oxide [34]. The layer thickness and dielectric function of the chemically grown oxide was kept constant in the analysis of the a-Si:H/c-Si heterojunctions. For structural characterization, transmission electron microscopy (TEM, Hitachi High-Tech Co., H-9500) and secondary ion mass spectroscopy (SIMS, ULVAC-PHI Inc., PHI ADEPT-1010) were used.

Electrons were accelerated with 200 kV in TEM measurements. In the SIMS measurements, the samples were irradiated by Cs^+ ions of 1.0 keV as primary ion species. The effective lifetime (τ_{eff}) and implied open circuit voltage (i-V_{OC}) were measured by quasi-steady-state photoconductance (Sinton Instruments, WCT-120) in 1/64 and transient mode [35,36]. We performed current versus voltage (I–V) measurements and obtained the resistance. An Al dot electrode with diameter of 1.5 mm was deposited on the front side, while the rear was fully covered by Al. Hydrogen depth profiles were obtained by NRA via the resonant $^1H(^{15}N,\alpha\gamma)^{12}C$ reaction. The $^{15}N^{2+}$ ion beam of 50-100 nA was generated by the MALT van de Graaff tandem accelerator at the University of Tokyo [26]. The γ-rays were collected by scintillation detectors. The errors bars of the charge-normalized γ-ray yields ΔI_{norm} were computed by the following equation:

$$\Delta I_{\mathrm{norm}} = \sqrt{I_{\mathrm{raw}} + R_{\mathrm{back}} \times t_{\mathrm{aq}}}/(I_{beam} \times t_{\mathrm{aq}}) \ , \quad (1)$$

where I_{norm}, I_{raw}, R_{back}, t_{aq}, and I_{beam} are charge-normalized γ-ray yield, raw γ-ray counts (γ-signal + background), background count rate, acquisition time, and ion beam current, respectively [26].

3. Results and Discussion

Figures 1(a) and 1(b) show τ_{eff} and i-V_{OC} of the as-deposited i-a-Si:H/n-c-Si heterojunctions with and without H_2O_2 OPT, respectively. The layer thickness of the i-a-Si:H is about 19 nm. The solid lines in Fig.1 are given as visual guides. For the samples treated with 1% H_2O_2 solution, the τ_{eff} and i-V_{OC} slightly increases with increasing immersion time. The passivation performance of the i-a-Si:H/n-c-Si heterojunctions decreases with the immersion time in H_2O_2 solutions with concentrations higher than 2%. The best τ_{eff} of 2.9 ms and i-V_{OC} of 0.715 V were obtained with 2% H_2O_2 solution for 30 s of immersion, which implies a 2-fold increase in τ_{eff}

compared to heterojunctions without OPT. Our results suggest that the coverage and layer thickness of the interlayer are critical to enhance the passivation performance. It is reported that the coverage and layer thickness of the silicon oxide grown on c-Si(100) and c-Si(111) surfaces in the H_2O_2 solutions increase with increasing oxidation time up to a critical duration [37,38]. Furthermore, Aoyama *et al*. found that the chemical oxides on c-Si(100) and c-Si(111) formed by solutions such as H_2O_2 are nonuniform [39]. Hence, the superior passivation performance after short immersion times may be attributed to an i-a-Si:H layer on ultrathin and non-uniform SiO_x interlayers. We support this conjecture in the following.

Figure 2 shows a cross-sectional TEM image of the i-a-Si:H/n-c-Si heterostructure with OPT in 2% H_2O_2 for 30 s. Clearly, no closed silicon oxide layer is observed at the i-a-Si:H/n-c-Si heterointerface. To characterize the O concentration at the buried heterointerface, SIMS measurements were performed. Figure 3 shows the SIMS depth profiles of the oxygen concentration (C_O) and the silicon ion intensity (I_{Si}) in the i-a-Si:H/n-c-Si heterostructures with OPT in (a) 1% H_2O_2 for 30 s, (b) 2% H_2O_2 for 30 s, and (c) 16% for 5 min. The C_O peaks and I_{Si} fluctuates at around 18 nm. The fluctuation is possibly due to changes in the ionization rate of Si owing to variable values of C_O. The peak position of C_O is good agreement with the layer thickness of a-Si:H determined by SE as described below. The C_O peak values were 1.26×10^{21} cm^{-3} for (a), 1.64×10^{21} cm^{-3} for (b), and 5.01×10^{21} cm^{-3} for (c), respectively. The layer thickness was calculated by S_O/C_{SiO2}, where S_O is O areal density and C_{SiO2} is O concentration in SiO_2. The S_O values were derived from integrating the C_O peak as shown in Figure S2, while C_{SiO2} was assumed as 2.196 g/cm^3. The estimated layer thicknesses were 0.05 nm for (a), 0.07 nm for (b), and 0.22 nm for (c), respectively. In this calculation, we assumed the silicon oxide layer prepared by OPT to be SiO_2, which means that the exceedingly small thickness values obtained from the SIMS measurements suggest that the OPT synthesized silicon oxide is of low-density and uneven on the c-Si surface. Therefore, based on the TEM images and SIMS

depth profiles, we consider that non-uniform and low-density SiO_x is formed by OPT, and that the uniformity and density are likely to increase during OPT with higher H_2O_2 concentrations and longer immersion times.

Figures 4(a) and 4(b) show *n* and *k* spectra of the as-deposited i-a-Si:H/n-c-Si heterojunctions without OPT, with OPT in 2% H_2O_2 for 30 s and with OPT in 16% H_2O_2 for 5 min. The layer thickness of the i-a-Si:H is approximately 19 nm. The dependence of the effective carrier lifetime on the minority carrier density (MCD) is shown in Figure S3. The τ_{eff} at MCD of 1×10^{15} cm^{-3}, i-V_{OC}, thickness of the a-Si:H ($t_{a\text{-}Si:H}$) layer, thickness of silicon oxide interlayer (t_{int}) and mean square error (MSE) of the SE analysis are summarized in Table I. The MSE values are about 1.3, meaning the applied optical model is reasonable (Supporting Information Figure S4). The OPT with more concentrated H_2O_2 solution and longer immersion time results in larger t_{int} due to enhanced oxidation of the c-Si surface. In Table I, the $t_{a\text{-}Si:H}$ is also seen to slightly increase by employing higher H_2O_2 concentrations and longer immersion times. As aforementioned, it is considered that the SiH_3 radical is the most dominant precursor for a-Si:H film formation [40,41]. In addition, excess H atoms are released and the hydrogen content reaches the steady state value of bulk a-Si:H during the growth [42]. Ramalingam *et al.* performed atomistic simulations and remarked that the H coverage on the surface, i.e. the dangling bond density, determines the reactivity between SiH_3 radicals and the c-Si surface [43]. We speculate that the sticking probability of SiH_3 radicals on H-terminated Si is smaller than that on SiO_x, so that different degrees of oxidation of the c-Si substrates may affect the final a-Si:H film thickness.

From the *n*-*k* spectra in Figure 4, an increase of *n* and *k* is observed for pre-oxidized samples, suggesting that less deficient and denser a-Si:H layers are formed [33,44]. Fourier-transform infrared measurements revealed that denser a-Si:H is mainly composed of monohydrides and

contains few microscopic voids [45]. Further, larger dielectric functions are observed for monohydride-dominated a-Si:H [33]. Hence, the increased n and k observed in Fig. 4 suggest that monohydrides in a-Si:H are dominant and that few micro-voids exist by employing OPT. The presumed increase in sticking probability of SiH_3 radicals on oxidized patches of the c-Si substrates may enhance the precursor attachment in the initial growth stage of a-Si:H, which would account for the slight increase in $t_{a\text{-}Si:H}$ and formation of denser a-Si:H layers.

NRA hydrogen profiling was performed for samples with and without OPT. Figure 5(a) shows NRA γ-ray yield curves of the c-Si substrates without H_2O_2 pre-oxidation and with OPT in either 2% H_2O_2 for 30 s or in 16% H_2O_2 for 5 min. These samples reflect the substrate conditions prior to deposition of the a-Si:H layers. The solid curves are fitting results using Gaussian functions. The peak intensity, peak position, and full width half maximum (FWHM) are given in Table II. From Table II, the γ-ray yield maximum at the 6.385 MeV resonance energy (indicative of surface H) decreased after OPT in 16% H_2O_2 for 5 min. The γ-ray yield after OPT in 2% H_2O_2 for 30 s is as same as that after OPT in 16% H_2O_2 for 5 min within the experimental accuracy. Hence, the number of H atoms on the c-Si surface is clearly reduced by OPT. Furthermore, a very slight peak shift to higher energy and increase in FWHM is observed after OPT in 2% H_2O_2 for 30 s and 16% H_2O_2 for 5 min, suggesting that a part of the H atoms is located closely below the surface. The layer thickness of the silicon oxide formed by OPT gradually increased and saturated after a duration of 300 s (Supporting Information Figure S5). From the SE analysis, the layer thickness of the silicon oxide was 9.1 Å and 11.8 Å for OPT using 2% H_2O_2 for 30 s and 16% H_2O_2 for 5 min, respectively. The layer thickness values were different from those calculated by SIMS depth profiles, which is possibly caused by an enhanced oxidation before the SE measurements. Hypothetically, if all H in the sample was located only at the SiO_2/c-Si interface underneath a 1-nm-thick SiO_2 layer (without any H on the surface), the γ-yield would peak at a ^{15}N ion energy of 6.3868 MeV, which is higher

than the OPT-induced peak shift in Fig. 5(a). In the same way, the γ-yield would peak at a ^{15}N ion energy of 6.3854 MeV by assumption of a 2.2-Å-thick SiO_2 layer, which is in good agreement with the observed peak shift. It is known that silicon hydrides and silicon hydroxyl groups are contained in chemically grown oxide [39]. Therefore, the very small peak shift and the reduced γ-ray yield can be explained by the evolution of a thin sub-stoichiometric silicon oxide layer that contains hydrogen species. The H-terminated Si bonds on the surface are partially replaced with O-terminated Si bonds with increasing OPT duration, which is also suggested by the SIMS depth profiles in Fig. 3. Furthermore, partial Si back-bond oxidation and concomitant formation of buried Si-OH species might also contribute to the observed small peak shift.

Figure 5(b) shows NRA γ-ray yield curves as a function of the incident $^{15}N^{2+}$ ion energy measured for as-deposited i-a-Si:H/n-c-Si heterojunctions with and without OPT. The $t_{\text{a-Si:H}}$ values of the samples are ~19 nm. Figure 5(c) shows a magnified part of Figure 5(b) in the ion energy range from 6.404 to 6.424 MeV. The surface of i-a-Si:H/n-c-Si corresponds to 6.385 MeV. The solid, dotted, and chain lines in Fig. 5(c) represent the positions of the a-Si:H/c-Si, the a-Si:H/SiO_x, and the SiO_x/c-Si interfaces, respectively. These a-Si:H/SiO_x/c-Si interface positions are reflected by the inflection point locations in the high energy falling edges of the NRA γ-yield curves (as obtained by sigmoid curve fitting, Supporting Information Figure S6) and are in good agreement with the $t_{\text{a-Si:H}}$ values determined by the SE analysis. No significant differences of the γ-ray yield are observed in the energy region from 6.385 to 6.405 MeV, which means that the H content in the bulk of the a-Si:H layers is the same within experimental accuracy. Compared with the sample without OPT, slightly higher γ-ray yields are observed at the a-Si:H/SiO_x and SiO_x/c-Si interfaces in Fig. 5(c) for the samples with OPT. The respective increases in a-Si:H layer thickness of 0.6 and 1.0 nm by OPT with 2% and 16% H_2O_2 are

significantly larger than the uncertainty of SE to determine $t_{\text{a-Si:H}}$ (±0.04 nm). The latter corresponds to an unmeasurably small difference of ^{15}N ion energy (0.06 keV), meaning that the respective interface positions are rather accurately defined on the ^{15}N energy axis of Fig. 5(c). Note that reduced γ-ray yields were observed on the oxidized substrate surfaces in Fig. 5(a), which means that the increased γ-ray yield near the a-Si:H/SiO_x heterointerfaces in Fig. 5(c) does not originate from H originally contained in the silicon oxide layers prior to deposition of a-Si:H. We can therefore conclude that the OPT causes a higher abundance of hydrogen atoms at the i-a-Si:H/SiO_x/n-c-Si heterointerfaces that are formed during a-Si:H deposition. Although no significant difference in γ-ray yields around the i-a-Si:H/SiO_x/n-c-Si heterointerfaces is observed between the OPT samples treated with 2% and 16% H_2O_2, the passivation performance of the sample treated with 2% H_2O_2 was remarkably superior. One possible reason for this is a different coverage of the SiO_x interlayer. As discussed above, the coverage of the c-Si surface by the SiO_x layer formed by OPT with 16% H_2O_2 is likely to be higher in comparison with that after OPT with 2% H_2O_2. In general, the passivation effect of ultra-thin SiO_x layers is poor, whereas that of the i-a-Si:H layer is good. As shown in Fig. 2, a SiO_x interlayer synthesized by OPT with 2% H_2O_2 was not apparent, indicating that the passivation effect is dominated by the i-a-Si:H layer on the n-c-Si substrate. Therefore, after OPT in 16% H_2O_2 for 5 min, a larger part of the c-Si surface is covered by a still thin SiO_x layer, which leads to inferior passivation properties.

Thin i-a-Si:H of less than ~5 nm thickness is of particular interest as it promises to achieve good passivation performance and effective carrier transport perpendicular to the i-a-Si:H/n-c-Si heterointerface. Thus, i-a-Si:H/n-c-Si heterojunctions with $t_{\text{a-Si:H}}$ values below 19 nm were characterized in order to clarify the influence of the i-a-Si:H layer thickness on the electrical performance of the heterojunctions. We also evaluated the effect of additional PDA processing. Figure 6(a) and 6(b) shows the layer thickness dependence of τ_{eff} and i-V_{OC} of i-a-Si:H/n-c-Si

heterojunctions with and without OPT using 2% H_2O_2 for 30 s. The $t_{a\text{-}Si:H}$ values of the samples with the interlayer are slightly larger than those of the samples without the interlayer. For the samples with i-a-Si:H films thicker than 8 nm, the τ_{eff} was increased after PDA. Higher τ_{eff} and i-V_{OC} values are obtained for the samples with the interlayer before and after PDA at 200 °C. The samples with the 4-nm-thick i-a-Si:H layer show a different behavior. Here, the passivation performance was improved after PDA (by a factor of ~1.5 in τ_{eff}) only for the sample with the interlayer. On the contrary, for the 4-nm-thick i-a-Si:H/n-c-Si heterojunction without the interlayer, the passivation performance degraded strongly after PDA.

To investigate the impact of the SiO_x interlayer on electrical conduction, current–voltage (*I–V*) measurements were carried out. Figure 6(c) shows *I–V* characteristics of n-a-Si:H/i-a-Si:H layers on n-c-Si with and without OPT. For the OPT, 2% H_2O_2 was employed for different treatment times. The thicknesses of the n-a-Si:H and i-a-Si:H layers are 5.0 nm and 6.5 nm, respectively. Linear *I–V* characteristics were observed for all samples. The electrical resistance values derived from linear regressions are shown in Figure 6(d). Almost identical resistances were observed for the heterojunction without OPT and with OPT for times shorter than 120 s, whereas the resistance increased after OPT for 5 min. Depending on the impurity concentration in SiO_2, the resistance of a 1-nm-thick SiO_2 layer ranges in the order of 10^1 to 10^7 Ω in our electrode configuration, which is much higher than the observed resistances of the heterojunctions. This supports our above conclusion that the chemically grown silicon oxide interlayer formed in 2% H_2O_2 is non-uniform SiO_x. These results show moreover that OPT with 2% H_2O_2 up to about 30 s enhances the passivation performance without a decrease in electrical conductivity.

Figure 7 shows NRA γ-ray yield curves measured for the ~4-nm-thick i-a-Si:H/n-c-Si heterojunctions (a) with and (b) without OPT as a function of the incident ^{15}N ion energy for

samples before and after PDA. The surface position corresponds to 6.385 MeV. The solid, dotted, and chain lines in Fig. 7 represent the positions of the a-Si:H/c-Si, the a-Si:H/SiO_x, and the SiO_x/c-Si interfaces for as-deposited samples, respectively. A 32.5% larger γ-ray yield profile is observed for the as-deposited sample with a SiO_x interlayer in comparison with the as-deposited sample that has no interlayer. Furthermore, the γ-ray yield at the SiO_x/c-Si interface in Fig. 7(a) and at the a-Si:H/c-Si interface in Fig 7(b) are almost identical, whereas the γ-ray yield at the a-Si:H/SiO_x interface becomes higher. These results confirm the findings of Fig. 5(b) and 5(c), namely that high quality a-Si:H layers are formed in presence of the SiO_x interlayer which appears to prevent hydrogen from desorbing in the initial stage of a-Si:H growth, leading to superior passivation performance. Moreover, Fig. 7 shows that the γ-ray yield of the samples with the interlayer is evidently maintained after PDA. De Wolf *et al.* suggested that the PDA-induced enhancement in passivation performance is caused by a rearrangement of hydrogen bonding states around the a-Si:H/c-Si heterointerface [22]. In light of our results that indicate no loss of interfacial H during PDA from OPT samples with 4-nm-thick a-Si:H layer, such a mechanism of PDA-induced enhancement of the passivation performance appears plausible. On the other hand, the γ-ray yield of the sample without the interlayer decreased after PDA, whereas the γ-ray yield at the a-Si:H/c-Si interface remained unchanged. This result suggests that partial desorption of hydrogen from the interface and from the a-Si:H layer occurred during PDA. It has been suggested that promotion of crystallization during PDA is responsible for the degradation of the passivation performance [12]. However, no significant decrease of $t_{\text{a-Si:H}}$ is observed for ~4-nm-thick a-Si:H/c-Si heterojunctions without the interlayer, which means that crystallization of the a-Si:H is not confirmed by our SE analysis. This conclusion is further supported by the NRA results. The interfacial inflection point in the H profile of the PDA-treated sample without the interlayer in Fig. 7 (b) does not

markedly shift to shallower depth, indicating that no significant shrinking of the a-Si:H layer takes place during PDA.

Further confirmation pending, we speculate that the residual Si dangling bonds in the slightly H-depleted thin (4 nm) PDA-treated a-Si:H layer in samples without OPT may act as trap sites for diffusible H atoms that are desorbed from the sensitive c-Si interface under light irradiation and thereby lead to a weakened passivation performance. Consistently, Figs. 6(a) and 6(b) suggest that this strongly detrimental effect of the PDA treatment on the passivation performance only prevails in the thinnest (4 nm) a-Si:H films, where the H-depleted surface-near region of the a-Si:H layer is rather close to the heterointerface, whereas samples with thicker a-Si:H layers are much less affected by this PDA-induced degradation.

4. Conclusion

We studied the impact of OPT and PDA on the passivation performance of and on the hydrogen distribution in i-a-Si:H/n-c-Si heterojunctions. A silicon oxide interlayer forms by immersing the c-Si substrates into H_2O_2 solutions prior to depositing the a-Si:H layer by means of PECVD. TEM images and SIMS depth profiles suggest that the silicon oxide interlayer prepared by OPT is non-uniform and of low-density. For 19-nm-thick a-Si:H, the τ_{eff} is improved from 1.3 to 2.9 ms and an enhancement of the i-V_{OC} by 3% is obtained under optimum OPT conditions (2% H_2O_2 solution for 30 s). For these OPT parameters, the SiO_x interlayer does not increase the electrical resistance of the heterojunctions. The dielectric functions analysed by SE suggest that less deficient and denser a-Si:H films are formed by inserting the SiO_x interlayers. NRA hydrogen profiling reveals a slightly higher near-interfacial H content in OPT-treated samples, whereas the H content in the bulk of the a-Si:H films is unaffected by

insertion of the SiO_x interlayer. The OPT becomes especially effective in case of thin a-Si:H layers, which are of particular practical interest as they promise good passivation performance and high carrier transport vertical to the heterointerface. For a-Si:H layers of less than 5 nm thickness, the optimized OPT process results in a 6-fold increased τ_{eff} and an improvement of i-V_{OC} by 11% compared with the PDA-treated heterostructure without the SiO_x interlayer. PDA (200 °C for 30 min) does not measurably change the near-interfacial H distribution in heterostructures with a 4 nm thick a-Si:H layer, but it causes a reduction of the H content in the surface-near region of the a-Si:H layer of i-a-Si:H/c-Si samples without OPT, whereas the H content in the a-Si:H layer of OPT-processed i-a-Si:H/SiO_x/c-Si heterostructure is stable during PDA. We conclude that the ultra-thin oxide interlayers can suppress hydrogen desorption from the near-surface region of the a-Si:H layer during the initial stage of film growth and during PDA, which results in less defective and thermally stable i-a-Si:H. These findings are informative for the fabrication of highly efficient silicon heterojunction solar cells with excellent passivation performance and high electrical conductivity.

CRediT authorship contribution statement

K.G. conceived the idea. K.G. carried out the sample preparation, electrical, optical characterization and analysis. K.G. and M.W. performed NRA measurements. M.W., S.O. and K.F assisted with conditioning the NRA system and analyzing the NRA results. M.W., S.O., Y.K., K.F and N.U. discussed the results. K.G. wrote the paper, and all other authors provided feedback.

Declaration of Interest Statement.

The authors declare that they have no known competing financial interests or personal relationships that could have appeared to influence the work reported in this paper.

Acknowledgements

This work was supported by New Energy and Industrial Technology Development Organization (NEDO) and MEXT, Grants-in-Aid for Scientific Research on Innovative Areas "Hydrogenomics", JP18H05514 and JP18H05518. We thank H. Miura and A. Shimizu for their technical supports.

Appendix A. Supplementary material

Supplementary materials to this article can be found at .

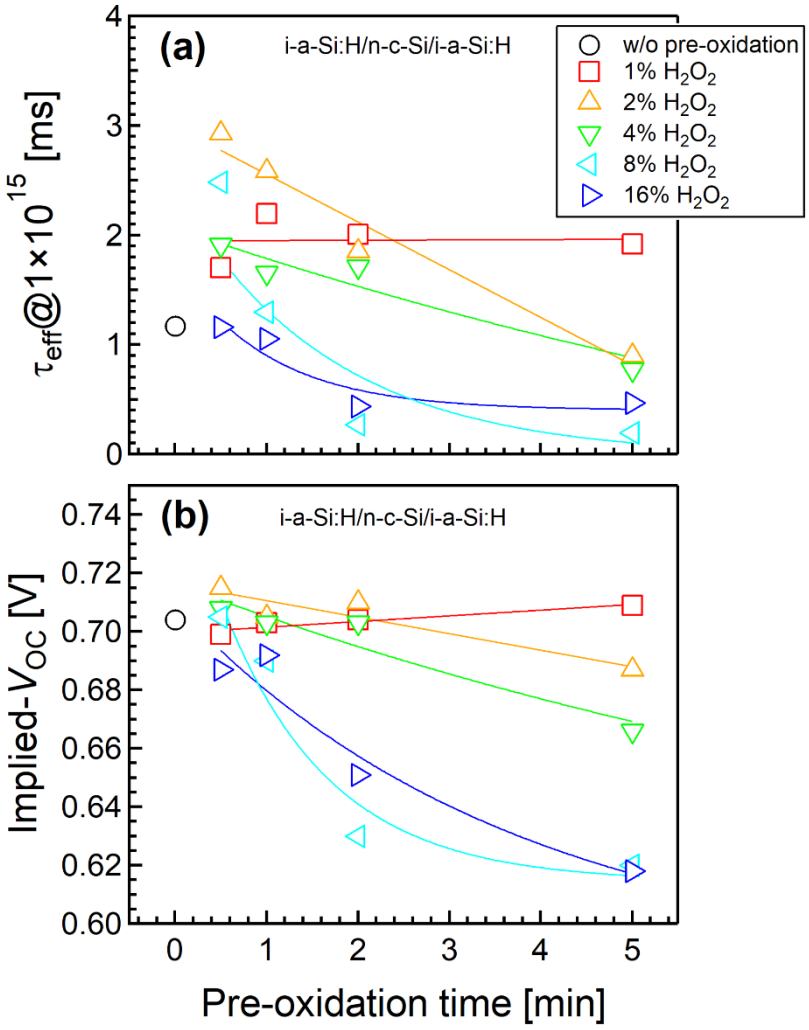

Figure 1. (a) τ_{eff} and (b) i-V_{OC} of the as-deposited i-a-Si:H/n-c-Si heterojunctions with and without oxidizing H_2O_2 pre-treatments. The layer thickness of i-aSi:H is about 19 nm. The solid lines are visual guides. (color online)

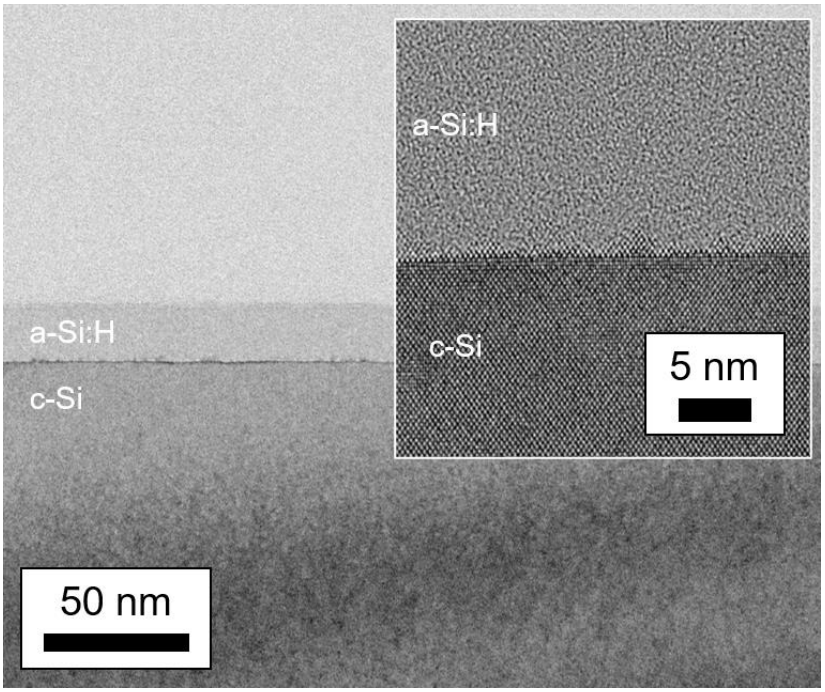

Figure 2. Cross-sectional TEM image of the as-deposited i-a-Si:H/n-c-Si heterojunction with oxidizing pre-treatment in 2% H_2O_2 for 30 s. The inset shows a magnification of the interfacial region.

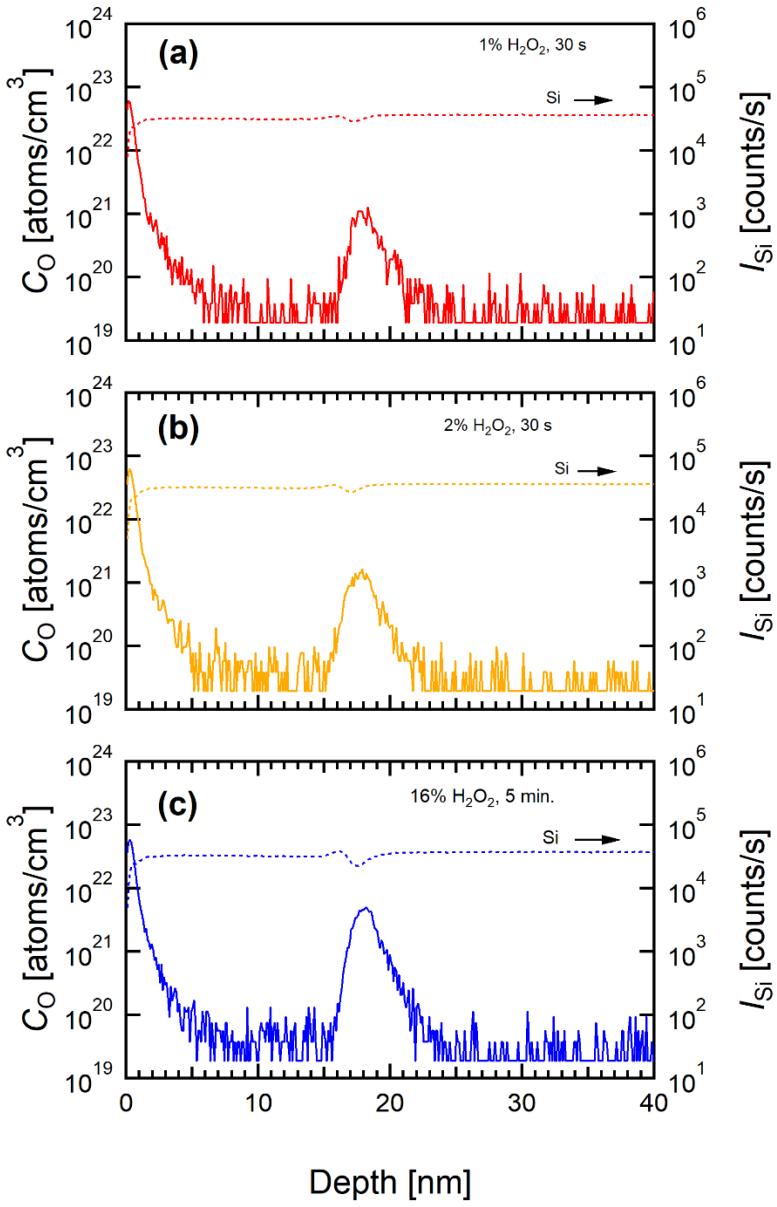

Figure 3. SIMS depth profiles of the i-a-Si:H/n-c-Si heterostructures with OPT in (a) 1% H_2O_2 for 30 s, (b) 2% H_2O_2 for 30 s, and (c) 16% for 5 min.

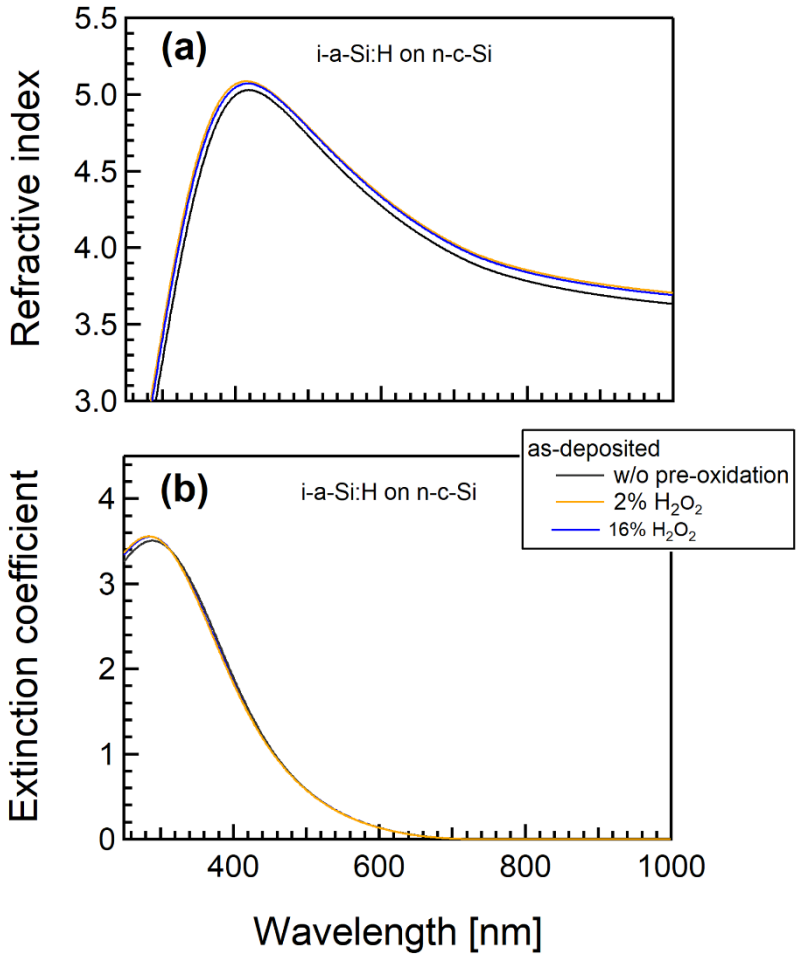

1

2 **Figure 4.** (a) Refractive index and (b) extinction coefficient spectra of as-deposited i-a-Si:H/n-

3 c-Si heterojunctions without H_2O_2 pre-oxidation, with oxidation in 2% H_2O_2 for 30 s and 16%

4 H_2O_2 for 5 min. (color online)

5

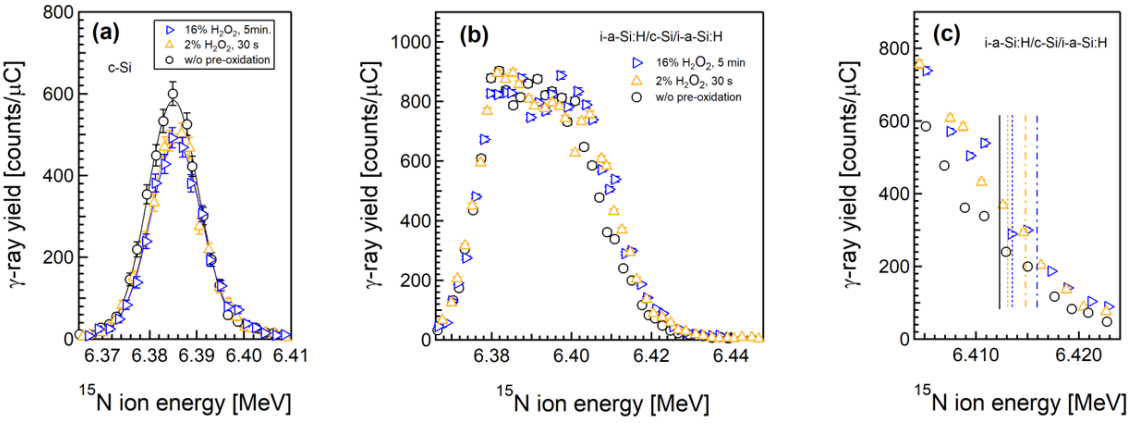

Figure 5. (a) NRA γ-ray yield curves of the c-Si substrates without pre-oxidation, with pre-oxidation in 2% H_2O_2 for 30 s and in 16% H_2O_2 for 5 min. The solid lines are fit curves to Gaussian functions. (b) NRA γ-ray yield curves of the a-Si:H/c-Si heterojunctions without H_2O_2 pre-oxidation, with pre-oxidation in 2% H_2O_2 for 30 s and in 16% H_2O_2 for 5 min. (c) Magnified graph in the ion energy range from 6.404 to 6.424 MeV. The surface position of i-a-Si:H/n-c-Si corresponds to 6.385 MeV. The solid, dotted, and chain lines represent the position of the a-Si:H/c-Si, the a-Si:H/SiO_x, and the SiO_x/c-Si interfaces, respectively, as determined by SE analyses. (color online)

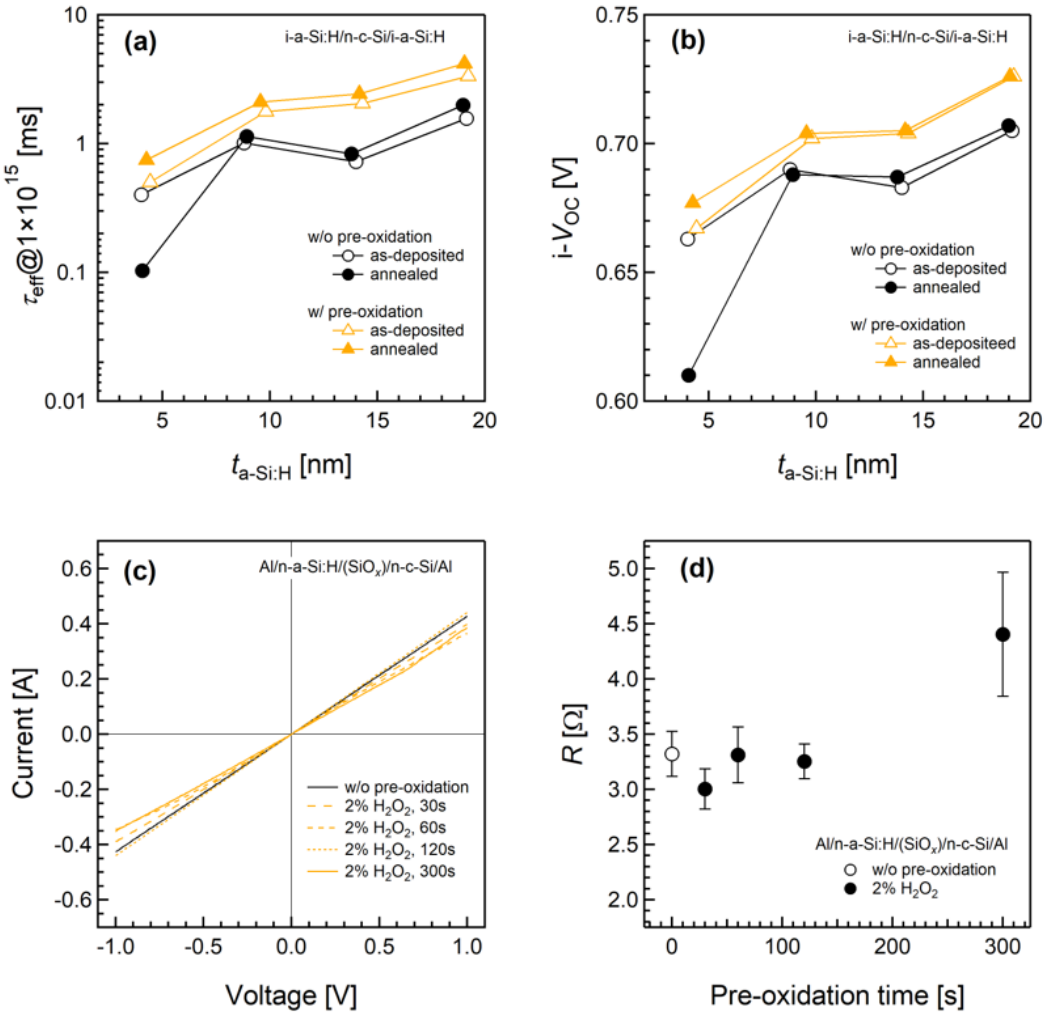

Figure 6. (a) τ_{eff} and (b) i-V_{OC} of the i-a-Si:H/n-c-Si heterojunctions with and without 2% H_2O_2 pre-oxidation treatments for 30 s as a function of the layer thickness of a-Si:H. (c) Current–voltage characteristics of the n-a-Si:H on n-c-Si heterojunctions. (d) Dependence of electrical resistance of the n-a-Si:H on n-c-Si heterojunctions on pre-oxidation time. (color online)

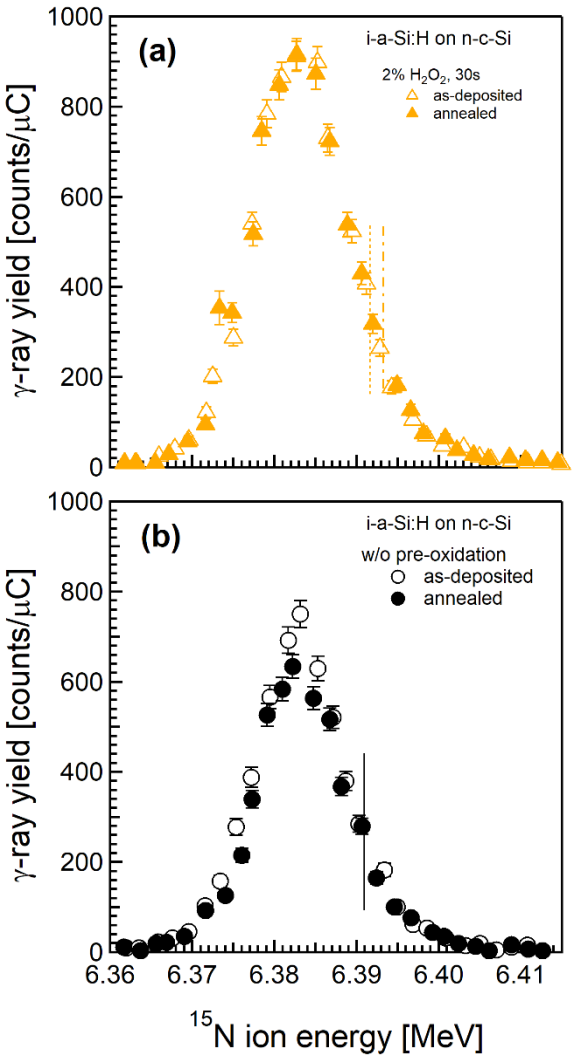

Figure 7. NRA γ-ray yield curves measured for as-deposited and PDA-treated i-a-Si:H/n-c-Si heterojunctions (a) with and (b) without pre-oxidation treatment (OPT). The $t_{\text{a-Si:H}}$ is about 4 nm, which means the a-Si:H/c-Si heterointerfaces corresponds to about 6.389 MeV. The solid, dotted, and chain lines represent the positions of the a-Si:H/c-Si, the a-Si:H/SiO_x, and the SiO_x/c-Si interfaces of the as-deposited samples, respectively. These interfacial positions are determined by SE analyses. (color online)

Table I. Effective lifetime, implied V_{OC}, layer thickness of a-Si:H layer, layer thickness of the silicon oxide interlayer, mean square error of SE analysis.

Oxidizing pre-treatment	τ_{eff} [ms]	i-V_{OC} [V]	$t_{a\text{-}Si:H}$ [nm]	t_{int} [nm]	MSE
w/o pre-oxidation	1.3	0.704	19.1 ± 0.04	–	1.23
2% H_2O_2 solution for 0.5 min	2.9	0.715	19.7 ± 0.04	0.9 ± 0.01	1.28
16% H_2O_2 solution for 5 min	0.2	0.618	20.1 ± 0.04	1.18 ± 0.01	1.31

Table II. The peak intensity, peak position, and full width half maximum (FWHM) of the c-Si substrates without H_2O_2 pre-oxidation and with OPT in either 2% H_2O_2 for 30 s or in 16% H_2O_2 for 5 min.

Oxidizing pre-treatment	Peak intensity [counts/μC]	Peak position [MeV]	FWHM [keV]
w/o pre-oxidation	571.9 ± 6.0	6385.0 ± 0.1	7.6 ± 0.1
2% H_2O_2 solution for 0.5 min	491.0 ± 9.1	6385.5 ± 0.1	7.7 ± 0.2
16% H_2O_2 solution for 5 min	468.2 ± 7.8	6385.6 ± 0.1	7.7 ± 0.2

REFERENCES

1. K. Yoshikawa, H. Kawasaki, W. Yoshida, T. Irie, K. Konishi, K. Nakano, T. Uto, D. Adachi, M. Kanematsu, H. Uzu, K. Yamamoto, Silicon Heterojunction Solar Cell with Interdigitated Back Contacts for a Photoconversion Efficiency over 26%, Nat. Energy 2 (2017) 17032.

2. K. Yoshikawa, W. Yoshida, T. Irie, H. Kawasaki, K. Konishi, H. Ishibashi, T. Asatani, D. Adachi, M. Kanematsu, H. Uzu, K. Yamamoto, Exceeding Conversion Efficiency of 26% by Heterojunction Interdigitated Back Contact Solar Cell with Thin Film Si Technology, Sol. Energy Mater. Sol. Cells 173 (2017) 37-42.

3. K. Yamamoto, K. Yoshikawa, H. Uzu, D. Adachi, High-efficiency Heterojunction Crystalline Si Solar Cells, Jpn. J. Appl. Phys. 57 (2018) 08RB20.

4. D. Adachi, J.L. Hernández, K. Yamamoto, Impact of Carrier Recombination on Fill Factor for Large Area Heterojunction Crystalline Silicon Solar Cell with 25.1% Efficiency, Appl. Phys. Lett. 107 (2015) 233506.

5. E. Kobayashi, S. De Wolf, J. Levrat, A. Descoeudres, A. Despeisse, F-J. Haug, C. Ballif, Increasing the Efficiency of Silicon Heterojunction Solar Cells and Modules by Light Soaking, Sol. Energy Mater. Sol. Cells 173 (2017) 43-49.

6. L. Korte, E. Conrad E, H. Angermann, R. Stangl, M. Scmidt, Advances in a-Si:H/c-Si Heterojunction Solar Cell Fabrication and Characterization, Sol. Energy Mater. Sol. Cells 93, (2009) 905-910.

7. M. Tanaka, M. Taguchi, T. Matsuyama, T. Sawada, S. Tsuda, S. Nakano, H. Hanafusa, Y. Kuwano, Development of New a-Si/c-Si Heterojunction Solar Cells: ACJ-HIT (Artificially Constructed Junction-Heterojunction with Intrinsic Thin-Layer), Jpn. J. Appl. Phys. 31, (1992) 3518-3522.

8. C. Leendertz, R. Stangl, T.F. Schulze, M. Schmidt, L. Korte, A Recombination Model

for a-Si:H/c-Si Heterostructures, Phys. Status Solidi C 7 (2010) 1005–1010.

9. S. Olibet, E. Vallat-Sauvain, C. Ballif, Model for a-Si:H/c-Si Interface Recombination Based on the Amphoteric Nature of Silicon Dangling Bonds, Phys. Rev. B 76 (2007) 035326.
10. M. Garín, U. Rau, W. Brendle, I. Martín, R. Alcubilla, Characterization of a-Si:H/c-Si Interfaces by Effective-lifetime Measurements, J. Appl. Phys. 98 (2005) 093711.
11. K. Gotoh, M. Wilde, S. Kato, S. Ogura, Y. Kurokawa, K. Fukutani, N. Usami, Hydrogen Concentration at a-Si:H/c-Si Heterointerfaces – The Impact of Deposition Temperature on Passivation Performance, AIP Advances 9 (2019) 075115.
12. S. De Wolf and M. Kondo, Abruptness of a-Si:H/c-Si Interface Revealed by Carrier Lifetime Measurements, Appl. Phys. Lett. 90 (2007) 042111.
13. H. Fujiwara and M. Kondo, Impact of Epitaxial Growth at the Heterointerface of a-Si:H/c-Si Solar Cells, Appl. Phys. Lett. 90 (2007) 013503.
14. J. Bian, L. Zhang, W. Guo, D. Wang, F. Meng, Z. Liu, Improved Passivation Effect at the Amorphous/crystalline Silicon Interface due to Ultrathin SiO_x Layers Pre-formed in Chemical Solutions, Appl. Phys. Exp. 7 (2014) 065504.
15. T. Oikawa, K. Ohdaira, K. Higashimine, H. Matsumura, Application of Crystalline Silicon Surface Oxidation to Silicon Heterojunction Solar Cells, Curr. Appl. Phys. 15 (2015) 1168-1172.
16. K. Ohdaira, T. Oikawa, K. Higashimine, H. Matsumura, Suppression of the Epitaxial Growth of Si Heterojunction Solar Cells by the Formation of Ultra-thin Oxide Layers, Curr. Appl. Phys. 16 (2016) 1026-1029.
17. A. Cuevas, Y. Wan, D. Yan, C. Samundsett, T. Allen, Z. Zhang, J. Cui, J. Bullock, Carrier Population Control and Surface Passivation in Solar Cells, Sol. Energy Mater. Sol. Cells 184 (2018) 38-47.

18. S. De Wolf, A. Descoeudres, Z.C. Holman, C. Ballif, High-efficiency Silicon Heterojunction Solar Cells: A Review, Green 2 (2012) 7-24.
19. A. Desccoeudres, L. Barraud, S. De Wolf, B. Strahm, D. Lachenal, C. Guérin, Z.C. Holman, F. Zicarelli, B. Demaurex, J. Seif, J. Holovsky, C. Ballif, Improved Amorphous/crystalline Silicon Interface Passivation by Hydrogen Plasma Treatment, Appl. Phys. Lett. 99 (2011) 123506.
20. T.F. Schulze, H.N. Beushausen, C. Leendertz, A. Dobrich, B. Rech, L. Korte, Interplay of Amorphous Silicon Disorder and Hydrogen Content with Interface Defects in Amorphous/crystalline Silicon Heterojunctions, Appl. Phys. Lett. 96 (2010) 252102.
21. S. De Wolf and M. Kondo, Nature of Doped a-Si:H/c-Si Interface Recombination, J. Appl. Phys. 105 (2009) 103707.
22. S. De Wolf, S. Olibet, C. Ballif, Stretched-exponential a-Si:H/c-Si Interface Recombination Decay, Appl. Phys. Lett. 93 (2008) 032101.
23. S. De Wolf and M. Kondo, Boron-doped a-Si:H/c-Si Interface Passivation: Degradation Mechanism, Appl. Phys. Lett. 91 (2007) 112109.
24. M. Wilde and K. Fukutani, Hydrogen Detection near Surfaces and Shallow Interfaces with Resonant Nuclear Reaction Analysis. Surf. Sci. Rep. 69 (2014) 196-295.
25. K. Fukutani, Below-surface Behavior of Hydrogen Studied by Nuclear Reaction Analysis, Curr. Opin. Solid State Mater. Sci. 6 (2002) 153-161.
26. M. Wilde, S. Ohno, S. Ogura, K. Fukutani, H. Matsuzaki, Quantification of Hydrogen Concentrations in Surface and Interface Layers and Bulk Materials through Depth Profiling with Nuclear Reaction Analysis, J. Vis. Experiments 109 (2016) 53452.
27. A. Moldovan, A. Fischer, J. Temmler, M. Bivour, T. Dannenberg, D. Erath, A. Lorenz, D. Sontag, J. Zhao, A.Wissen, F. Clement, M. Zimmer, J. Rentsch, Recent Developments in the Industrial Silicon Heterojunction Process Chain Enabling Efficiencies up to 22.7%, Energy Procedia 124 (2017) 357-364.

28. A. Moldovan, T. Dannenberg, J. Temmler, L. Kroely, M. Zimmer, J. Rentsch, Ozone-based Surface Conditioning Focused on an Improved Passivation for Silicon Heterojunction Solar Cells, Energy Procedia 92 (2016) 374-380.
29. H. Angermann K. Wolke, C. Gottschalk, A. Moldovan, M. Roczen, J. Fittkau, M. Zimmer J. Rentsch, Electronic Interface Properties of Silicon Substrates after Ozone Based Wet-chemical Oxidation Studied by SPV Measurements, Appl. Surf. Sci. 258 (2012) 8387-8396.
30. D. Chen, L. Zhao, H. Diao, W. Zhang, G. Wang, W. Wang, Low-temperature Sintering Properties of the Screen-printed Silver Paste for a-Si:H/c-Si Heterojunction Solar Cells, J. Mater. Sci: Mater. Electron. 25 (2014) 2657-2664.
31. L. Serenelli, M. Miliciani, M. Izzi, R. Chierchia, A. Mittiga, M. Tucci, Advances in Screen Printing Metallization for a-Si:H/c-Si Heterojunction Solar Cells. IEEE Photovolt. Special. Conf. Proc. (2014) 2528-2532.
32. G.E. Jellison Jr and F.A. Modine, Parameterization of the Optical Functions of Amorphous Materials in the Interband Region, Appl. Phys. Lett. 69 (1996) 371-373.
33. S. Kageyama, M. Akagawa, H. Fujiwara, Dielectric Function of a-Si:H Based on Local Network Structures, Phys. Rev. B 83 (2011) 195205.
34. G.E. Jellison, Examination of Thin SiO_2 Films on Si Using Spectroscopic Polarization Modulation Ellipsometry, J. Appl. Phys. 69 (1991) 7627-7634.
35. A. Cuevas and R. Sinton, Prediction of the Open-circuit Voltage of Solar Cells from the Steady-state Photoconductance, Prog. Photovolt. Res. Appl. 5 (1997) 79-90.
36. R. Sinton and A. Cuevas, Contactless Determination of Current‐voltage Characteristics and Minority-carrier Lifetimes in Semiconductors from Quasi-steady-state Photoconductance Data. Appl. Phys. Lett. 69 (1996) 2510-2512.
37. M. Morita, T. Ohmi, E. Hasegawa, A. Teramoto, Native Oxide Growth on Silicon Surface in Ultrapure Water and Hydrogen Peroxide, Jpn. J. Appl. Phys. 29 (1990) L2392-L2394.

38. U. Neuwald, A. Feltz, U. Memmert, R.J. Behm, Chemical Oxidation of Hydrogen Passivated Si(111) Surfaces in H_2O_2, J. Appl. Phys. 78 (1995) 4131-4136.
39. T. Aoyama, T. Yamazaki, T. Ito, Nonuniformities in Chemical Oxides on Silicon Surfaces Formed during Wet Chemical Cleaning, J. Electrochem. Soc. 143 (1996) 2280-2285.
40. J.R. Abelson, Plasma Deposition of Hydrogenated Amorphous Silicon: Studies of the Growth Surface, Appl. Phys. A56 (1993) 493-512.
41. N. Itabashi, N. Nishiwaki, M. Magane, T. Goto, A. Matsuda, C. Yamada, E. Hirota, SiH_3 Radical Density in Pulsed Silane Plasma, Jpn. J. Appl. Phys. 29 (1990) 585-590.
42. A. Terakawa and H. Matsunami, Hydrogen Elimination Model of the Formation of Hydrogen Bonding Structures during the Growth of Hydrogenated Amorphous Silicon by Plasma CVD, Phys. Rev. B 62 (2000) 16808.
43. S. Ramalingam, D. Maroudas, E.S. Aydil, Atomistic Simulation Study of the Interactions of SiH_3 Radicals with Silicon Surfaces, J. Appl. Phys. 86 (1999) 2872-2888.
44. J.P. Seif, A. Descoeudres, M. Filipič, F. Smole, M. Topič, Z.C. Holman, S. De Wolf, C. Ballif, Amorphous Silicon Oxide Window Layers for High-efficiency Silicon Heterojunction Solar Cells, J. Appl. Phys. 115, (2014) 024502.
45. A.H.M. Smets, W.M.M. Kessels, and M.C.M. van de Sanden, Vacancies and voids in hydrogenated amorphous silicon, Appl. Phys. Lett. 82, (2003) 1547-1549.]

1 Supplementary Materials

2

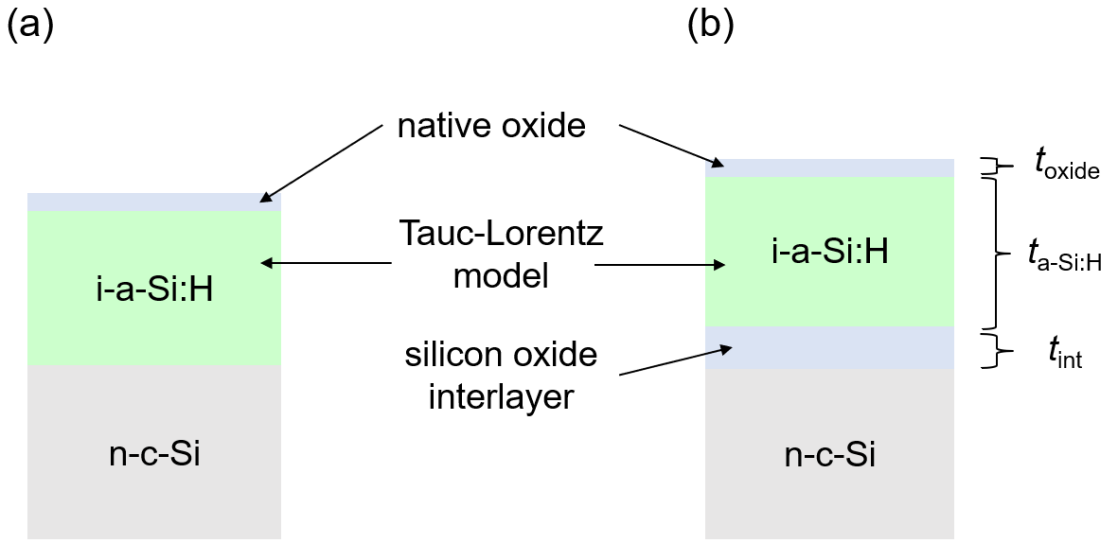

3

4 **Figure S1**: Schematic structure of the optical models for (a) a-Si:H/c-Si and (b) a-Si:H/SiO_x/c-

5 Si heterojunctions. For modeling silicon oxide, the Sellmeier model [Reference] was used.

6

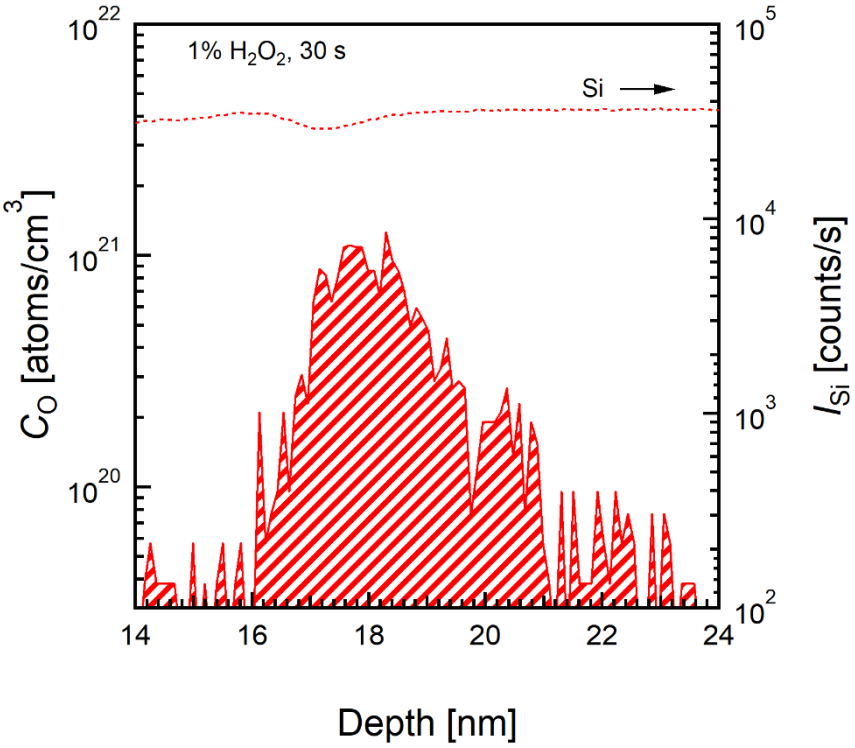

Figure S2: SIMS depth profile of the i-a-Si:H/n-c-Si heterojunction with oxidation in 1% H_2O_2 for 30 s. The O areal density (S_O) was calculated from the oxygen concentration integrated within the hatched area.

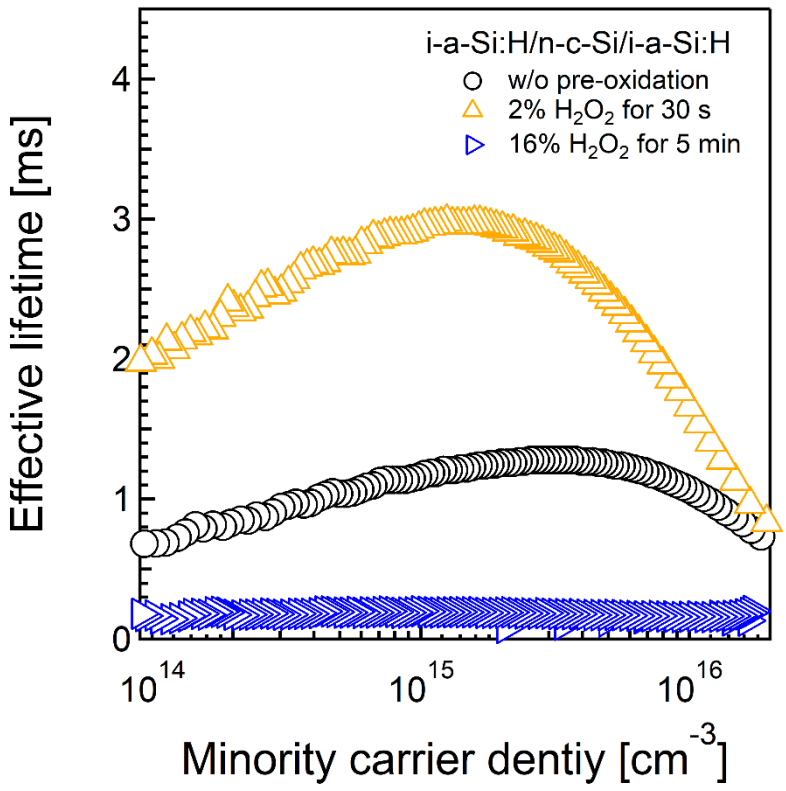

Figure S3: Effective carrier lifetime vs minority carrier density of the i-a-Si:H/n-c-Si heterojunctions without H_2O_2 pre-oxidation, with oxidation in 2% H_2O_2 for 30 s, and 16% H_2O_2 for 5 min.

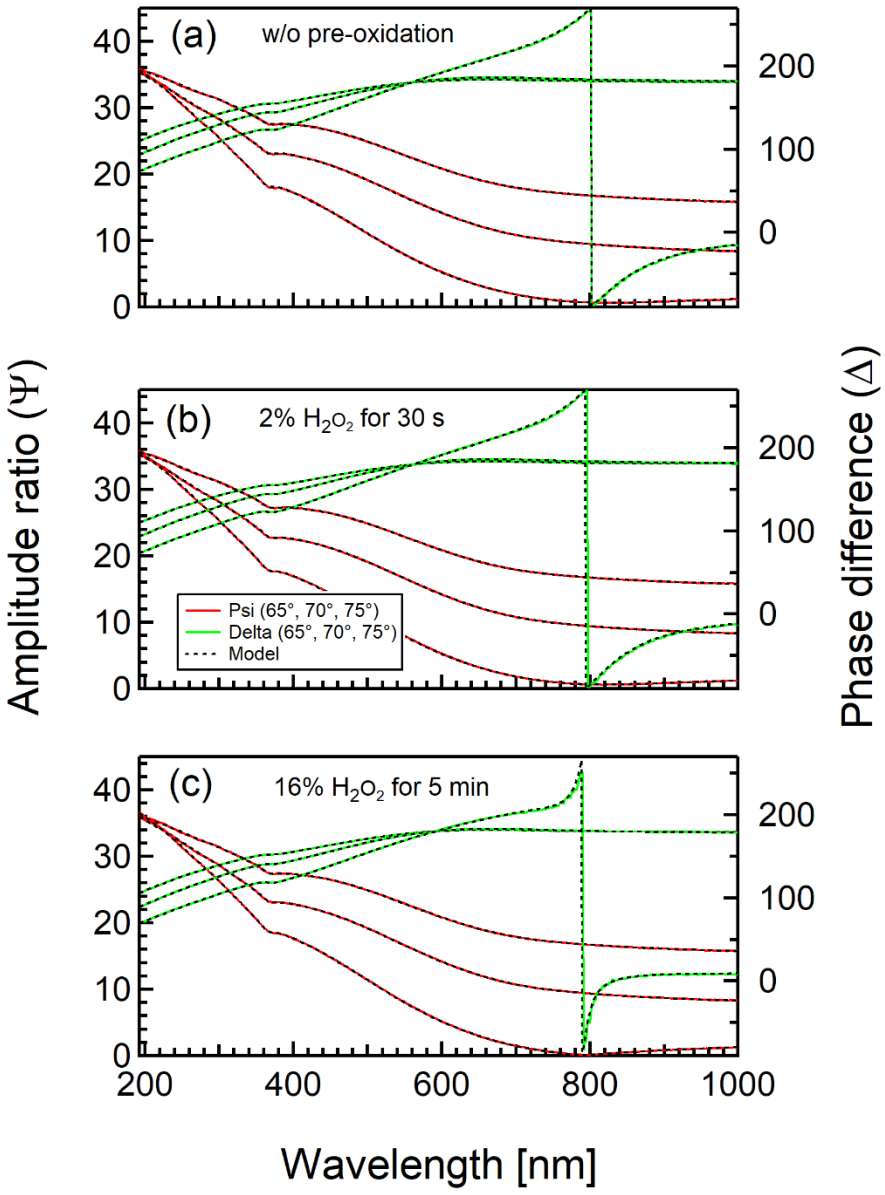

1

2 **Figure S4**: Amplitude ratio and phase difference spectra of the i-a-Si:H/n-c-Si heterojunctions
3 without H_2O_2 pre-oxidation (a), and with oxidation in 2% H_2O_2 for 30 s (b) and 16% H_2O_2 for
4 5 min (c).

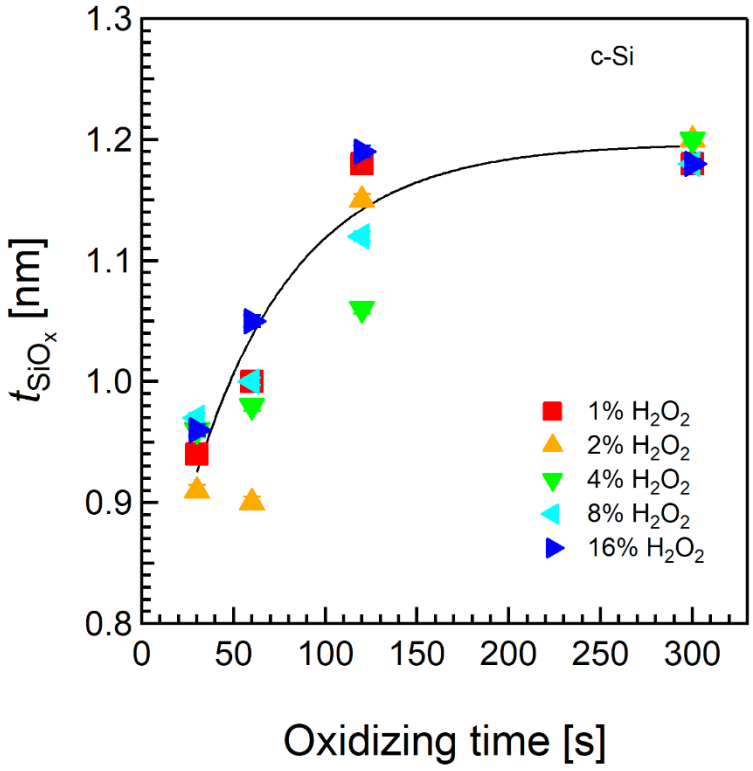

1

2 **Figure S5**: Layer thickness of silicon oxide on c-Si as a function of the H_2O_2 oxidizing time.

3

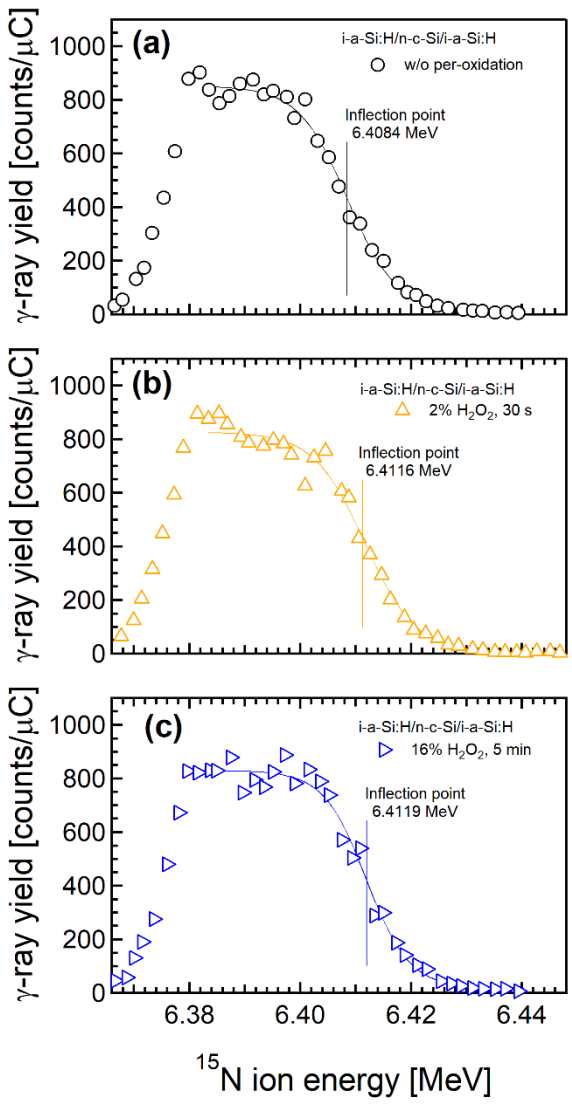

Figure S6: NRA γ-ray yield curves of the a-Si:H/c-Si heterojunctions (a) without H_2O_2 pre-oxidation, with (b) pre-oxidation in 2% H_2O_2 for 30 s and (c) in 16% H_2O_2 for 5 min. The inflection points are determined by fitting the respective data with sigmoid functions (solid lines).